Time-Dependent Resilience in the Presence of Interacting Multiple Hazards in a Changing Climate

Cao Wang, Ph.D., M.ASCE[1]; Bilal M. Ayyub, Ph.D., P.E., Dist.M.ASCE[2]; Hao Zhang, Ph.D., M.ASCE[3]; and Michael Beer, Dr.Eng., M.ASCE[4]

Abstract: The safety and serviceability of in-service structures and infrastructure systems are often threatened by natural hazards. Asset owners/decision makers are thus concerned about the resilience of an object of interest (structure or infrastructure), that is, its ability to be in readiness for, to absorb, recover from, and adapt to disruptive events. This is particularly the case when considering the potential impacts of climate change, which may lead to nonstationary natural hazards in the future (e.g., increasing wind hazard in a changing climate). Moreover, in many occasions, the presence of concurrent multiple hazards may result in more severe performance reduction to structures/infrastructures, compared with the occurrence of single hazards. This paper proposes an innovative method for the time-dependent resilience assessment of structures and infrastructure systems exposed to the impacts of concurrent multiple hazards in a changing climate. The interaction between different types of hazards is reflected through the mutual dependency between the performance functions associated with these hazards. New insights into the time-dependent resilience problem are also provided through a new concept of the performance concern index (PCI). It is shown that the mean nonresilience (i.e., 1 minus the mean value of resilience), if small enough, can be approximated by the mean value of the average PCI over the time domain of interest. Two examples are presented to demonstrate the applicability of the proposed method, and to investigate the sensitivity of resilience to key factors such as the interaction between multiple hazards and the climate change scenario. **DOI: 10.1061/AOMJAH.AOENG-0024**. © *2023 American Society of Civil Engineers*.

Author keywords: Time-dependent resilience; Multiple hazards; Hazard interaction; Climate change; Performance concern index.

Introduction

Natural hazards such as earthquakes and tropical cyclones (hurricanes) are among the major threatening factors for the safety and serviceability of civil structures and infrastructure systems during their service lives (Gerstenberger et al. 2020; Wang et al. 2020). Fragility, reliability, and resilience have been widely used tools to measure an object's (e.g., an individual structure or an infrastructure system consisting of multiple facilities) ability to withstand the effects of hazardous events. Of these quantities, the fragility model evaluates the conditional occurrence probability of a particular damage state (e.g., collapse) on a given intensity measure (Reed et al. 2016; Gidaris et al. 2017; Argyroudis et al. 2019). Reliability analysis takes into account the uncertainty associated with the resistance as well as that of the hazard intensity, yielding a fully probabilistic assessment of the object's state – survival or failure (Ayyub and McCuen 2016; Melchers and Beck 2018; Wang 2021; Wang et al. 2021). The concept of resilience, compared with reliability, additionally incorporates the recovery process of an object in the aftermath of a disruptive event, and is typically measured by the integral of performance function within a reference period of interest (Bruneau and Reinhorn 2007; McAllister 2013; Ayyub 2015; Salomon et al. 2020). With this regard, a dimensionless measure for resilience, denoted by R_e, was proposed by Attoh-Okine et al. (2009) as follows:

$$R_e = \frac{1}{t_2 - t_1}\int_{t_1}^{t_2} Q(t)\,dt \tag{1}$$

where $Q(t)$ is the functionality/performance function of the object at time t, taking a value between 0 and 1, t_1 is the occurrence time of a hazardous (disruptive) event, and t_2 is the time to full recovery (or a user-defined reference time; see, e.g., Cimellaro et al. 2010). Note that the resilience model in Eq. (1) cannot fully reflect the sensitivity of resilience to the variation of performance function. To overcome this disadvantage, a generalized resilience measure takes the following form (Wang 2023a):

$$R_e = f^{-1}\left[\frac{1}{t_2 - t_1}\int_{t_1}^{t_2} f(Q(t))\,dt\right] \tag{2}$$

where $f(x)$ ($x \in [0, 1]$) is a monotonic generating function. If $f(x) \equiv x$, then Eq. (2) reduces to Eq. (1). It was shown by Wang (2023a) that, with a properly selected $f(x)$ (e.g., $f(x) = \ln x$), the mean value of R_e in Eq. (2) is mathematically equivalent to reliability, and thus

[1]Vice-Chancellor's Postdoctoral Research Fellow, School of Civil, Mining, Environmental and Architectural Engineering, Univ. of Wollongong, Wollongong, NSW 2522, Australia (corresponding author). ORCID: http://orcid.org/0000-0002-2802-1394. Email: wangc@uow.edu.au

[2]Professor and Director, Center for Technology and Systems Management, Dept. of Civil and Environmental Engineering, Univ. of Maryland, College Park, MD 20742; Co-Director, International Joint Research Center for Resilient Infrastructure, Tongji Univ., Shanghai 200092, China. ORCID: https://orcid.org/0000-0003-2692-241X. Email: ba@umd.edu

[3]Associate Professor, School of Civil Engineering, The Univ. of Sydney, Sydney, NSW 2006, Australia. Email: hao.zhang@sydney.edu.au

[4]Professor of Uncertainty in Engineering and Head, Institute for Risk and Reliability, Leibniz Univ. Hannover, Hannover 30167, Germany; Professor, Institute for Risk and Uncertainty, Univ. of Liverpool, Liverpool L69 7ZF, UK; Guest Professor, International Joint Research Center for Resilient Infrastructure and International Joint Research Center for Engineering Reliability and Stochastic Mechanics, Tongji Univ., Shanghai 200092, China. Email: beer@irz.uni-hannover.de

Note. This manuscript was submitted on August 30, 2023; approved on October 19, 2023; published online on December 1, 2023. Discussion period open until May 1, 2024; separate discussions must be submitted for individual papers. This paper is part of the ***ASCE OPEN: Multidisciplinary Journal of Civil Engineering***, © ASCE, ISSN 2995-4266.

establishes a unified framework for reliability and resilience analyses.

The performance function $Q(t)$ is essentially affected by the hazardous events. Many types of natural hazards display nonstationary characteristics in terms of occurrence frequency and/or magnitude due to the potential impacts of climate change (IPCC 2021). For example, Walsh et al. (2016) projected that the future wind hazard will decrease in Northern Australia, but will increase along the East Coast. Xu et al. (2020) reported that, in a changing climate, most climate models considered in their study (five of six) result in a significantly shortened return period of tropical cyclone winds over the 21st century for Hangzhou and Shanghai – two coastal cities in China. For California, Goss et al. (2020) found that the state-wide increase in temperature and decrease in precipitation over the past four decades have contributed to the increasing aggregate fire weather indices. Relevantly, the ATSE (2022) recently released a position statement, summarizing that "Planning and design for resilience is a key component in mitigating the damage of major hazards and the effects of climate change."

In many occasions, in-service structures and infrastructures are exposed to the impacts of concurrent multiple hazards (Yin and Li 2011; Wahl et al. 2015; Salman and Li 2017; Bruneau et al. 2017), instead of single hazard types. One example is that, in August 2023, the state of California was hit by Hurricane Hilary and a magnitude-5.1 earthquake on the same day during the state's wildfire season (CalMatters 2023), prompting the necessity of considering the effects of multiple hazards for the region. The interdependencies of the hazard-induced damaging effects on structures and infrastructures need to be adequately addressed in resilience assessment. Ouyang et al. (2012) proposed a multistage framework for the resilience assessment of infrastructure networks, with a focus on the "expected annual resilience metric" for both single hazard types and concurrent multiple hazards. They also presented a case study on the resilience of a power transmission grid in Harris County, Texas. Li et al. (2020) presented a framework for resilience and loss assessment of highway bridges in the presence of multiple independent natural hazards, including earthquakes, hurricanes, and floods. They employed a stochastic renewal process to describe the random occurrence of hazardous events. Wang et al. (2022) developed a mathematical formula for the time-dependent resilience assessment of aging structures in a changing climate. They treated the occurrence of different types of hazards as statistically independent, and used a Poisson process to model the occurrence of hazards. However, these works did not consider the impact of mutual dependency between different hazards on resilience. Further, Laurien et al. (2022) reviewed 17 representative approaches to climate and disaster resilience measurement, and revealed the lack of existing resilience approaches that account for the interactions of multiple hazards. Moreover, it was stated by the Risk and Resilience Measurement Committee (2019, Chapter 4) that, "The effect of multiple hazards on infrastructure response is not explicitly considered in current codes and standards, and the nonstationarity of hazards (e.g., due to climate change) is also seldom considered." This observation motivates the development of novel analytical approaches that address the resilience problem (of, e.g., individual structures, infrastructure systems, or communities) considering the concurrence of multiple hazards and the potential impacts of climate change.

The aim of this paper is to develop a novel approach for resilience assessment of structures and infrastructure systems that are subjected to multiple hazards in a changing climate. The method benefits from the resilience model in Eq. (2) with the generating function being $f(x) = \ln x$, and takes into account the mutual dependency of performance functions associated with different hazard types. New insights into the resilience problem are also provided through proposing a new concept of the "performance concern index," which measures the asset owner/decision maker's concern arising from nonfull performance of structures or infrastructure systems. The applicability of the proposed resilience method is illustrated through two examples. The impacts of influencing factors, such as the mutual dependency between different hazards, the climate change scenario, and the recovery profiles in the aftermath of hazardous events, on time-dependent resilience are investigated through sensitivity analyses. Focusing on the resilience of structures and infrastructure systems, the scope of this paper is related to the UN Sustainable Development Goal 11, which is themed "making cities and human settlements inclusive, safe, resilient and sustainable."

Resilience Measure

Resilience for a Single Hazard Type

Consider the time-dependent resilience of an object (structure or infrastructure) within a reference period of $[0, t_l]$, denoted by $R_e(0, t_l)$. Extending the model in Eq. (2) with the generating function being $f(x) = \ln x$, the resilience is as follows (Wang 2023a):

$$R_e(0, t_l) = \exp\left[\frac{1}{t_l}\int_0^{t_l} \ln Q(t)dt\right] \tag{3}$$

Note that $R_e(0, t_l)$ in Eq. (3) has been based on the geometric mean of the performance function within the reference period of $[0, t_l]$. To demonstrate this point, subdivide $[0, t_l]$ into n identical intervals, namely $[0, t_l/n] \cup [t_l/n, 2t_l/n] \cup \cdots \cup [(n-1)t_l/n, t_l]$. Let Ω_i be the performance function evaluated at the midpoint of the ith interval for $i = 1, 2, \ldots, n$, that is, $\Omega_i = Q((i-0.5)T/n)$. From a view of Riemann integral, with a sufficiently large n, Eq. (3) becomes

$$R_e(0, t_l) = \lim_{n\to\infty} \exp\left[\frac{1}{n}\sum_{i=1}^{n} \ln \Omega_i\right] = \lim_{n\to\infty}\left(\prod_{i=1}^{n} \Omega_i\right)^{1/n} \tag{4}$$

which is the geometric mean of the sequence $\Omega_1, \Omega_2, \ldots, \Omega_n$. Note that the resilience model in Eq. (1) (or its extended form to a reference period of $[0, t_l]$ by replacing t_1, t_2 with 0, t_l, respectively) has been based on the arithmetic mean of the performance function. A key feature of Eq. (3), compared with arithmetic mean-based resilience, is that it can better reflect the sensitivity of resilience to the variation of $Q(t)$. Illustratively, consider a structure with full performance (i.e., $Q(t) = 1$) for the reference period of $[0, t_l/2]$; subsequently, due to the occurrence of a hazardous event at time $t_l/2$ causing collapse of the structure, the performance function reduces to zero in the absence of a resource that supports the recovery process (i.e., $Q(t) = 0$ for $t \in [t_l/2, t_l]$). In such a case, the structure is deemed as "nonresilient" with a zero value for resilience. This is consistent with Eq. (3). However, if applying an arithmetic mean-based resilience model [e.g., Eq. (1) with t_1, t_2 replaced by 0, t_l, respectively], the resilience is 0.5, suggesting that the structure is partially resilient.

It is further noticed that the performance function $Q(t)$ in Eq. (3) is a stochastic process by nature, with which $R_e(0, t_l)$ is a random variable. To achieve a scalar measure for resilience, the mean value of $R_e(0, t_l)$ in Eq. (3) is considered, denoted by $\overline{R}_e(0, t_l)$, which is evaluated according to

$$\overline{R}_e(0, t_l) = \mu\left\{\exp\left[\frac{1}{t_l}\int_0^{t_l} \ln Q(t)\, dt\right]\right\} \tag{5}$$

in which $\mu(\,)$ denotes the mean value of the variable in the brackets. In this following, the resilience model in Eq. (5) will be adopted,

where $\overline{R}_e(0, t_l)$ is referred to as mean resilience. The resilience assessment considering multiple hazards will be formulated in the next section.

Proposed Resilience Measure Considering Multiple Hazards

In the presence of totally m types of hazards, the individual performance associated with the ith hazard type is denoted by $Q_i(t)$ for $i = 1, 2, \ldots, m$. The integrated performance considering the combined effects of the m types of hazards, denoted by $Q_{\text{mul}}(t)$, is dependent on the joint behavior of $Q_1(t)$, $Q_2(t)$, …, $Q_m(t)$, and is expressed as follows based on a properly defined function ψ:

$$Q_{\text{mul}}(t) = \psi(Q_1(t), Q_2(t), \ldots, Q_m(t)) \tag{6}$$

It is expected that $Q_{\text{mul}}(t)$ takes a value between 0 and 1, and $Q_{\text{mul}}(t) \le Q_i(t)$ holds $\forall i$. In this paper, the following formulation of $Q_{\text{mul}}(t)$ is considered:

$$Q_{\text{mul}}(t) = \prod_{i=1}^{m} Q_i(t) \tag{7}$$

Note that Eq. (7) does not require statistical independence between the performance functions $Q_i(t)$. It is applicable to the general cases where the percentage of performance degradation due to a hazardous event is measured with respect to the existing performance of an object. The determination of each $Q_i(t)$ is dependent on the specific type of hazard and posthazard damage state of an object, and is generally representative of the asset owner/decision maker's attitude toward the hazard-induced residual performance.

One numerical example of applying Eq. (7) is presented in Fig. 1, considering two performance functions $Q_1(t)$ and $Q_2(t)$ corresponding to two hazard types. A Type 1 hazard occurs at time $t = 1$, and a Type 2 hazard occurs at time $t = 2$. The recovery duration in the aftermath of both events is 2 [i.e., from $t = 1$ to 3 in Fig. 1(a), and from $t = 2$ to 4 in Fig. 1(b)]. The integrated performance function, $Q_{\text{mul}}(t)$, is dependent on the joint behavior of $Q_1(t)$ and $Q_2(t)$, as depicted in Fig. 1(c). For example, when $t \in [2, 3]$, $Q_1(t) = Q_2(t) = 0.5$, yielding $Q_{\text{mul}}(t) = Q_1(t) \cdot Q_2(t) = 0.25$. Note that the graphs in Fig. 1 have been used herein for illustration purposes only. The dependence of performance function on the specific type of hazard will be later demonstrated in the "Examples" section.

Based on Eq. (5), replacing $Q(t)$ with $Q_{\text{mul}}(t)$ yields the resilience model in the presence of multiple hazards as

$$\overline{R}_{e,\text{mul}}(0, t_l) = \mu\left\{\exp\left[\frac{1}{t_l}\sum_{i=1}^{m}\int_0^{t_l} \ln Q_i(t)\, dt\right]\right\} \tag{8}$$

In Eq. (8), if each performance function $Q_i(t)$ is statistically independent, it follows that

$$\overline{R}_{e,\text{mul}}(0, t_l) = \prod_{i=1}^{m} \overline{R}_{e,i}(0, t_l) \tag{9}$$

in which $\overline{R}_{e,i}(0, t_l)$ is the mean resilience considering the ith hazard only [evaluated by substituting $Q_i(t)$ into Eq. (3)], $i = 1, 2, \ldots, m$. Eq. (9) suggests that, if not considering the mutual dependency between different hazard types, the mean resilience considering multiple hazards equals the multiplication of the mean resiliences associated with each hazard type. This observation is consistent with the results of Wang et al. (2022). Illustratively, for the three scenarios in Figs. 1(a–c), based on the three trajectories of performance function, the resiliences for [0, 6] are 0.794, 0.794, and 0.630, respectively (note that $0.794 \times 0.794 = 0.630$), according to Eq. (3).

Note that Eq. (9) does not necessarily hold if considering the mutual dependency between different performance functions. For the case in Fig. 1, at time $t = 2$ when the Type 2 hazard occurs, if the recovery process is postponed due to the recovery associated with the Type 1 hazard being in progress, and is resumed at $t = 3$, the "updated" performance function for the Type 2 hazard, denoted by $Q_2^*(t)$, is presented in Fig. 2(b). Correspondingly, the integrated performance function is affected by $Q_2^*(t)$, denoted by $Q_{\text{mul}}^*(t)$ (where the asterisk symbol accounts for the consideration of dependency of $Q_2(t)$ on $Q_1(t)$). The graph of $Q_{\text{mul}}^*(t)$, which equals $Q_1(t) \cdot Q_2^*(t)$, is plotted in Fig. 2(c).

Based on the trajectory in Fig. 2(c), the resilience over [0, 6] is evaluated according to Eq. (3) as 0.561. This is smaller than that associated with Fig. 1(c), implying the impact of performance function dependency on resilience.

Taking into account the mutual dependency between different performance functions, $Q_i(t)$ is modified as $Q_i^*(t)$ for $i = 1, 2, \ldots, m$ [$Q_i^*(t) \equiv Q_i(t)$ if the ith performance function is not affected by others; see, for example, $Q_1(t)$ in Fig. 2(a)], and Eq. (8) is rewritten as

$$\overline{R}_{e,\text{mul}}(0, t_l) = \mu\left\{\exp\left[\frac{1}{t_l}\sum_{i=1}^{m}\int_0^{t_l} \ln Q_i^*(t)\, dt\right]\right\} \tag{10}$$

Eq. (10) is the proposed method for resilience assessment in the presence of multiple hazards. It has been built on the

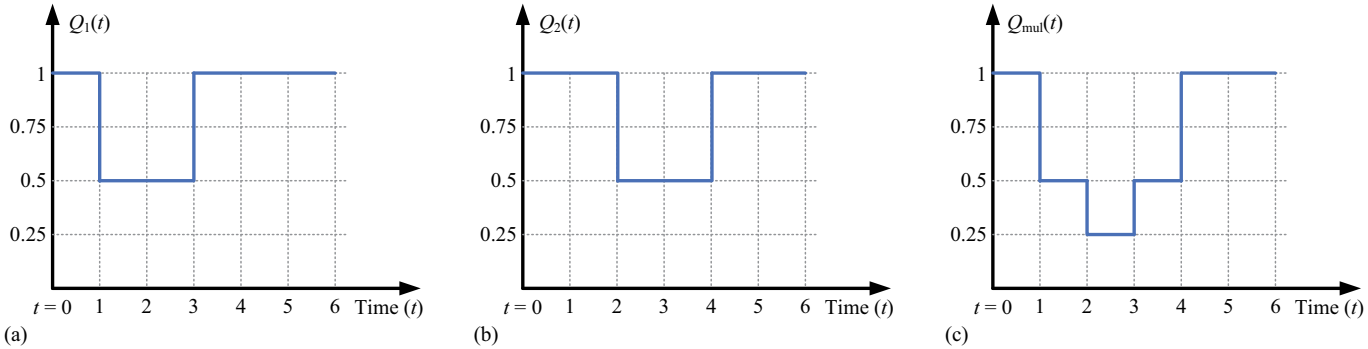

Fig. 1. Time variation of performance functions: (a) $Q_1(t)$; (b) $Q_2(t)$; and (c) $Q_{\text{mul}}(t)$.

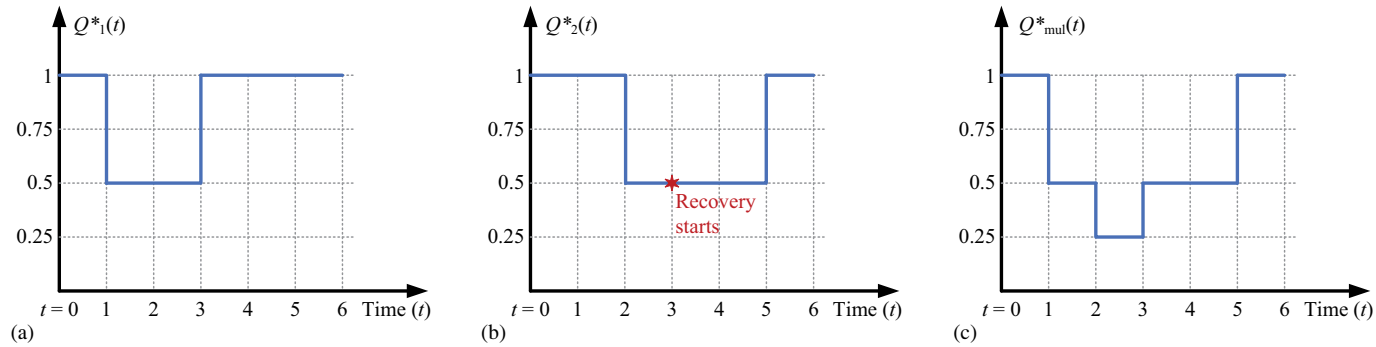

Fig. 2. Time variation of performance functions considering dependence of $Q_2(t)$ on $Q_1(t)$: (a) $Q^*_1(t)$; (b) $Q^*_2(t)$; and (c) $Q^*_{mul}(t)$.

multiplication-based definition of $Q_{mul}(t)$ in Eq. (7), and can be extended to fit other definitions in Eq. (6). Note that in Eq. (10), the consideration of climate change impacts on hazardous events can be reflected in the evaluation of each $Q^*_i(t)$, and subsequently in the resilience measure $\overline{R}_{e,mul}(0, t_l)$.

One can employ Monte Carlo simulation to evaluate Eq. (10) numerically. This requires to generate samples for the performance functions $Q^*_1(t)$, $Q^*_2(t)$, …, $Q^*_m(t)$. To this end, one can first discretize the reference period $[0, t_l]$ by subdividing it into n identical intervals, namely $[0, t_l/n] \cup [t_l/n, 2t_l/n] \cup \cdots \cup [(n-1)t_l/n, t_l]$. Let $\Omega_{i,j}$ denote the ith performance function evaluated at the midpoint of the jth interval for $i = 1, 2, \ldots, m$; $j = 1, 2, \ldots, n$, that is, $\Omega_{i,j} = Q_i((j-0.5)T/n)$. Denote $\Omega_{1,0} = \Omega_{2,0} = \cdots = \Omega_{m,0} = 1$. With an increasing j from 1 until n, one can determine $\Omega_{1,j}$, $\Omega_{2,j}$, …, $\Omega_{m,j}$ according to the values of $\Omega_{1,j-1}$, $\Omega_{2,j-1}$, …, $\Omega_{m,j-1}$ by incorporating the mutual dependency between different performance functions. Finally, substituting the generated trajectories of $Q^*_1(t)$, $Q^*_2(t)$, …, $Q^*_m(t)$ into Eq. (10) yields a sample resilience. Through N replications of simulation (where N is a sufficiently large integer), the mean value of the N sample resiliences converges to the mean resilience.

Discussion on the Kernel of Resilience Definition

The kernel of the resilience model in Eq. (10), $\sum_{i=1}^{m} \int_0^{t_l} \ln Q^*_i(t) dt$, has been built based on the logarithm of the performance functions. This is similar to the definition of the "Shannon information content" (a basic quantity in information theory), which is defined as follows for an outcome of x (MacKay 2003; Ayyub and Klir 2006):

$$\mathbb{I}(x) = -\ln p(x) \tag{11}$$

in which $p(x)$ is the occurrence probability of outcome x. An important feature of the information content $\mathbb{I}(x)$ is that, for two independent outcomes x and y, $\mathbb{I}(x, y) = \mathbb{I}(x) + \mathbb{I}(y)$, in which $\mathbb{I}(x, y)$ is the information content of the outcome (x, y) (i.e., the concurrence of x and y).

Similar to Eq. (11), a new concept of the "performance concern index" (PCI) is proposed in this paper, which measures asset owner/decision maker's concern about the performance of an object (structure or infrastructure), $Q(t)$. The PCI at time t, denoted by $\mathbb{C}(t)$, takes a form of

$$\mathbb{C}(t) = -\ln Q(t) = \ln \frac{1}{Q(t)} \tag{12}$$

The PCI in Eq. (12) satisfies the following conditions simultaneously.

1. A state of full performance (i.e., $Q(t) = 1$) leads to no concern.
2. A smaller value of $Q(t)$ means greater concern (i.e., $\mathbb{C}(t)$ is a monotonic function of $Q(t)$).
3. For two independent performance functions (corresponding to two independent hazard types), the total amount of concern equals the sum of the concerns associated with the individual performance functions.

To verify, it is straightforward to see that $\mathbb{C}(t)$ in Eq. (12) meet conditions (1) and (2). For condition (3), note that for two independent performance functions, namely $Q_1(t)$ and $Q_2(t)$, it follows that, $Q^*_{mul}(t) = Q_{mul}(t) = Q_1(t) \cdot Q_2(t)$. Thus, $\ln[1/Q^*_{mul}(t)] = \ln[1/Q_{mul}(t)] = \ln[1/Q_1(t)] + \ln[1/Q_2(t)]$. This indicates the additivity property (see definition in, e.g., Ayyub and Klir 2006) of the PCI in the presence of independent performance functions. For more general cases where $Q^*_{mul}(t) < Q_{mul}(t)$ (i.e., the dependency between individual performance functions worsens the integrated performance), it follows that $\ln[1/Q^*_{mul}(t)] > \ln[1/Q_1(t)] + \ln[1/Q_2(t)]$, with which the PCI is superadditive.

One can further show that there is a unique function that satisfies all the three conditions mentioned previously, up to a multiplicative scaling factor. Generally, let $g(x)$ denote such a function, that is, $\mathbb{C}(t) = g(Q(t))$. From condition (3), $g(Q_1(t) \cdot Q_2(t)) = g(Q_1(t)) + g(Q_2(t))$ holds for any performance functions $Q_1(t)$ and $Q_2(t)$. This further results in $g(x) = \alpha \ln x$, where α is a constant (see proof in, e.g., Milkman 1950). Next, since $g(x)$ is a decreasing function of x [see condition (2)], α is assigned a negative value [it equals -1 in Eq. (12)].

Denote $\mathbb{C}_{mul}(t) = -\ln Q_{mul}(t)$. The average PCI over $[0, t_l]$, $\overline{\mathbb{C}}_{mul}$, is evaluated according to

$$\overline{\mathbb{C}}_{mul} = \frac{1}{t_l} \int_0^{t_l} \mathbb{C}_{mul}(t)\, dt \tag{13}$$

Based on Eqs. (10) and (13), it follows that

$$\overline{R}_{e,mul}(0, t_l) = \mu\left[\exp\left(-\overline{\mathbb{C}}_{mul}\right)\right] \tag{14}$$

Eq. (14) establishes a simple relationship between the mean resilience and the average PCI; it provides a new angle to understand the resilience problem from asset owner/decision maker's concern about the performance function of an object (structure or infrastructure) over its life cycle. Let $\overline{nR}_{e,mul}(0, t_l)$ be the time-dependent mean nonresilience for a reference period of $[0, t_l]$, which equals $1 - \overline{R}_{e,mul}(0, t_l)$. An equivalent form of Eq. (14) is that

$$\overline{nR}_{e,mul}(0, t_l) = \mu\left[1 - \exp\left(-\overline{\mathbb{C}}_{mul}\right)\right] \tag{15}$$

Note that in Eq. (15), $\overline{\mathbb{C}}_{mul}$ varies from 0 to infinity. Correspondingly, the item $1 - \exp(-\overline{\mathbb{C}}_{mul})$ takes a value between 0 and 1, and thus can be treated as the "normalized" form of the average PCI. The mean value of the normalized $\overline{\mathbb{C}}_{mul}$ equals the mean nonresilience, which also varies within [0, 1].

In Eq. (15), if $\overline{\mathbb{C}}_{\text{mul}} \approx 0$ (i.e., a well-designed and maintained object that raises little concern), it follows that

$$\overline{\text{n}R}_{e,\text{mul}}(0, t_l) \approx \mu(\overline{\mathbb{C}}_{\text{mul}}) \tag{16}$$

Examples

Example 1: Impact of Performance Function Dependency on Mean Resilience

In this section, a numerical example, as adopted from Wang (2023b) with modification, is used to demonstrate the applicability of the proposed resilience model in Eq. (10), and to quantify the impact of performance function dependency on mean resilience.

Consider a structure subjected to two types of natural hazards, denoted by H1 and H2. The associated performance functions are $Q_1(t)$ and $Q_2(t)$, respectively. For simplicity, assume that the statistics of the hazards and their damaging effects on the structure are identical. For each hazard type, the occurrence is modeled by a nonstationary Poisson process with an occurrence rate of $\lambda(t) = c_0 + c_\lambda t$ (in year^{-1}), in which c_0 is the occurrence rate at the initial time, and c_λ is a constant representing the changing rate of $\lambda(t)$ (note that $c_\lambda = 0$ results in a stationary occurrence process of the hazards). Conditional on the occurrence of a hazardous event (either type) at time t, the remaining functionality (performance) becomes Q_r times the state immediately before the hazard occurrence. Assume that Q_r follows a Beta distribution with a mean value of $\mu_Q(t)$ (a function of time) and a coefficient of variation (COV) of 0.2. The recovery of functionality immediately after the occurrence of a hazardous event is linear. The recovery rate, K, is dependent on Q_r (i.e., the severity of performance reduction) and resourcefulness, and is expressed as $K = \xi \cdot (0.2 + 2Q_r)$ (in year^{-1}), in which ξ is a constant that reflects the resourcefulness for the recovery process. A reference period of 50 years is considered in this example.

To reflect the dependency between the two performance functions, $Q_1(t)$ and $Q_2(t)$, the following six types of dependency are considered.

i. Type 1, $Q_2(t)$ is affected by $Q_1(t)$ only: immediately after the occurrence of an H2 event causing reduced $Q_2(t)$, the recovery process is postponed if another recovery associated with H1 is in progress (until the completion of the H1-related recovery).
ii. Type 2, $Q_1(t)$ and $Q_2(t)$ affect each other: immediately after the occurrence of an Hi event causing reduced $Q_i(t)$ ($i = 1$, 2), the recovery process is postponed if another recovery associated with Hj ($j = 3 - i$) is in progress (until the completion of the Hj-related recovery).
iii. Type 3, $Q_2(t)$ is affected by $Q_1(t)$ only: immediately after the occurrence of an H2 event causing reduced $Q_2(t)$, the remaining functionality is further reduced by a factor of η_q if the instant $Q_1(t)$ is not in full performance.
iv. Type 4, $Q_1(t)$ and $Q_2(t)$ affect each other: immediately after the occurrence of an Hi event causing reduced $Q_i(t)$ ($i = 1$, 2), the remaining functionality is further reduced by a factor of η_q if the instant $Q_j(t)$ ($j = 3 - i$) is not in full performance.
v. Type 5, $Q_2(t)$ is affected by $Q_1(t)$ only: combining the effects in Types 1 and 3.
vi. Type 6, $Q_1(t)$ and $Q_2(t)$ affect each other: combining the effects in Types 2 and 4.

For visualization purposes, Fig. 3 presents a set of sampled trajectories of $Q_1(t)$, $Q_2(t)$, $Q_1^*(t)$, $Q_2^*(t)$, $Q_{\text{mul}}(t)$, $Q_{\text{mul}}^*(t)$ for a reference period of 50 years (note that $Q_{\text{mul}}^*(t) = Q_1^*(t) \cdot Q_2^*(t)$), considering Type 5 interaction between $Q_1(t)$ and $Q_2(t)$ (thus, $Q_1^*(t) \equiv Q_1(t)$). For the scenario in Fig. 3, $\eta_q = 0.7$ and $\xi = 1$ (i.e., it needs five months to fully restore a 50% functionality). The mean value of Q_r decreases linearly from 0.8 at the initial time to 0.3 by the end of 50 years, with which $\mu_Q(t) = 0.8 - 0.01t$, where t is in years. Over 50 years, there are six H1 events and seven H2 events, as depicted in Fig. 3. The dependency of $Q_2(t)$ on

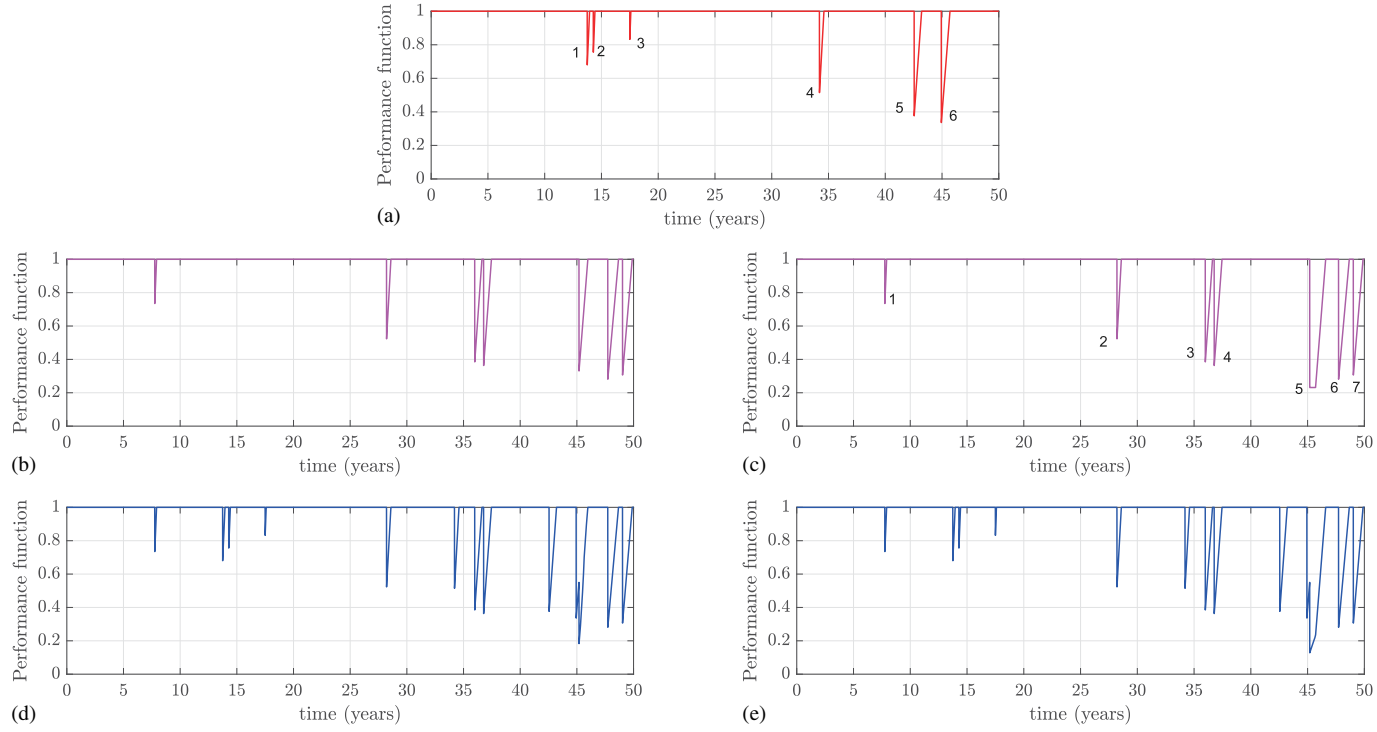

Fig. 3. Sampled trajectories of performance functions considering Type 5 interaction between $Q_1(t)$ and $Q_2(t)$: (a) $Q_1(t)$; (b) $Q_2(t)$; (c) $Q_2^*(t)$; (d) $Q_{\text{mul}}(t)$; and (e) $Q_{\text{mul}}^*(t)$.

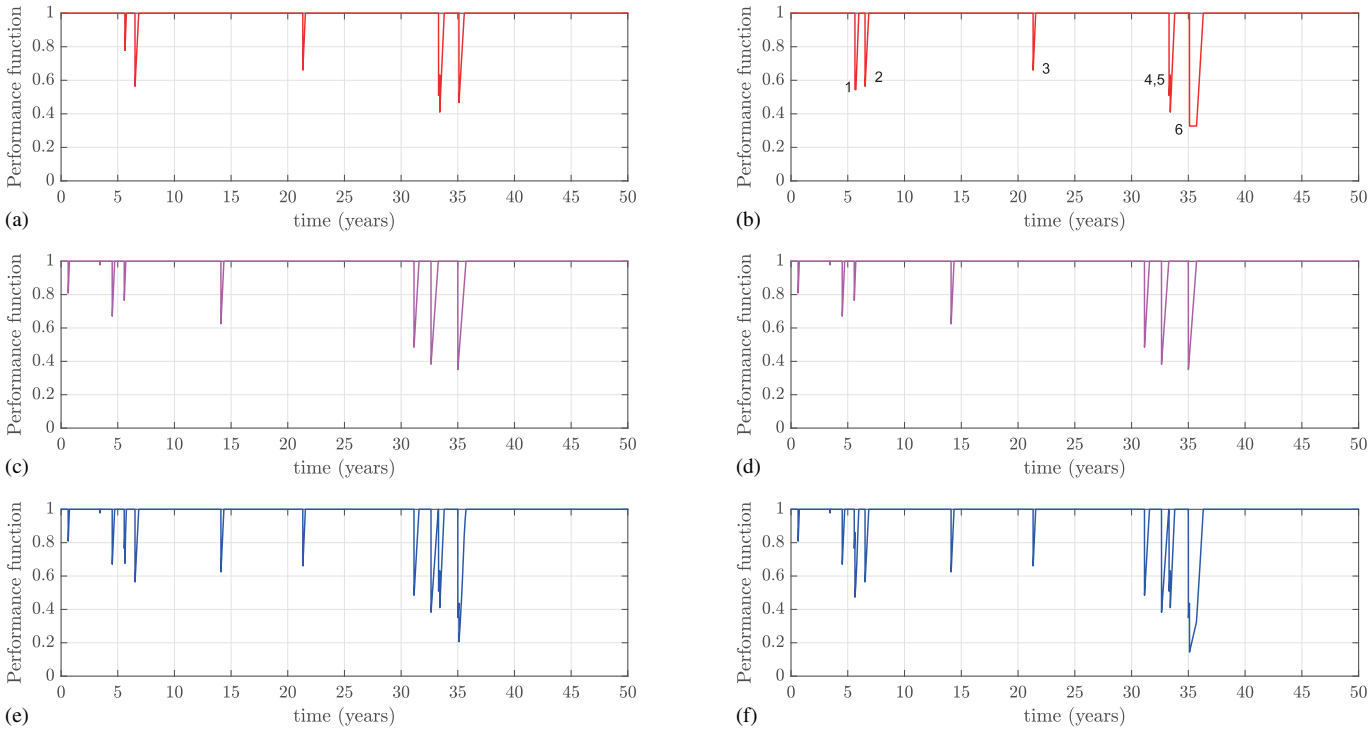

Fig. 4. Sampled trajectories of performance functions considering Type 6 interaction between $Q_1(t)$ and $Q_2(t)$: (a) $Q_1(t)$; (b) $Q_1^*(t)$; (c) $Q_2(t)$; (d) $Q_2^*(t)$; (e) $Q_{\text{mul}}(t)$; and (f) $Q_{\text{mul}}^*(t)$.

$Q_1(t)$ is reflected through the occurrence of the fifth H2 event [Fig. 3(c)], including: (1) the reduction of $Q_2(t)$ is further amplified due to the corresponding $Q_1(t)$ not in full performance, and (2) the recovery process is postponed due to the recovery associated with the sixth H1 event being in progress, and is resumed until the completion of the H1-related recovery. The updated $Q_2^*(t)$ further impacts the integrated performance function $Q_{\text{mul}}^*(t)$, as revealed through the comparison between Figs. 3(d and e).

Similar to Fig. 3, sample trajectories of the performance functions considering the Type 6 interaction between $Q_1(t)$ and $Q_2(t)$ are plotted in Fig. 4 (based on the same configuration as in Fig. 3). At the occurrence of the first and sixth H1 events, $Q_1(t)$ is affected by $Q_2(t)$ in terms of amplified performance deterioration and postponed recovery process. For example, the performance function associated with H1 reduces to 0.33 due to the sixth H1 event in Fig. 4(b), which is otherwise 0.47 with independent $Q_1(t)$ and $Q_2(t)$ [Fig. 4(a)]. This further explains the difference between $Q_{\text{mul}}(t)$ and $Q_{\text{mul}}^*(t)$ in Figs. 4(e and f).

The interaction between performance functions is also affected by the recovery profiles in the aftermath of hazardous events. Recall that $\xi = 1$ in Fig. 3. Sampled trajectories of the performance functions are depicted in Fig. 5 with $\xi_h = 0.2$ (i.e., it takes 25 months to restore functionality from 50% to 100%). With a longer duration of the recovery process, the Q_1–Q_2 interaction is enhanced. For example, as depicted in Fig. 5(d), the recovery process associated with the fourth H2 event is postponed significantly, due to the long hazard–restoration–hazard process associated with H1. Further, in Figs. 5(b and d), a hazardous event may occur before the full completion of the recovery process, with which the temporal correlation between the recovery profiles for the same hazard type arises (Wang 2023b).

Fig. 6 depicts the time-dependent mean nonresilience [evaluated according to Eq. (10)] for reference periods up to 50 years, considering Type 5 and 6 interactions of $Q_1(t)$ and $Q_2(t)$. The occurrence rate for both hazard types is modeled as $\lambda(t) = 0.1(1 + 0.01t)$, with which the occurrence rate increases by 50% over 50 years. The values of η_q and ξ are the same as those in Fig. 4. For comparison purposes, the mean nonresilience with independent $Q_1(t)$ and $Q_2(t)$ is also plotted in Fig. 6. It is observed that ignoring the performance function dependency will overestimate the resilience of an object, thus yielding a nonconservative evaluation. The mean nonresilience associated with Type 5 is smaller than that of Type 6, because Type 5 has partially considered the interaction between $Q_1(t)$ and $Q_2(t)$.

Recall that according to Eq. (16), if the mean nonresilience is close to zero, it can be approximated by the mean value of the average PCI. This can be verified by examining the case in Fig. 6. For a reference period of 50 years, the mean value of PCI equals 0.048 and 0.050 for Types 5 and 6, respectively (not shown in the figure), with a difference of only 2.86% and 3.04% compared with the corresponding mean nonresilience.

To investigate the impact of hazard nonstationarity in a changing climate on resilience, the dependence of mean nonresilience on $\lambda(t)$ and $\mu_Q(t)$ (reflecting the time variation of hazard magnitude conational on occurrence) for reference periods up to 50 years is presented in Fig. 7, considering the Type 6 interaction of $Q_1(t)$ and $Q_2(t)$. In Fig. 7(a), $c_0 = 0.1$, and the variation of c_λ represents different changing scenarios of the hazard occurrence rate. A greater value of c_λ results in larger mean nonresilience due to the greater accumulative risks for the structure, and this effect is amplified with a longer reference period. Fig. 7(b) examines four changing patterns for the time-variant mean value of Q_r, that is, $\mu_Q(t)$ decreases linearly from 0.8 at the initial time to 0.5, 0.4, 0.3, and 0.2, respectively, over 50 years. A more severe deterioration of the mean value of Q_r, which is representative of amplified hazard intensity over time due to climate change, leads to greater mean

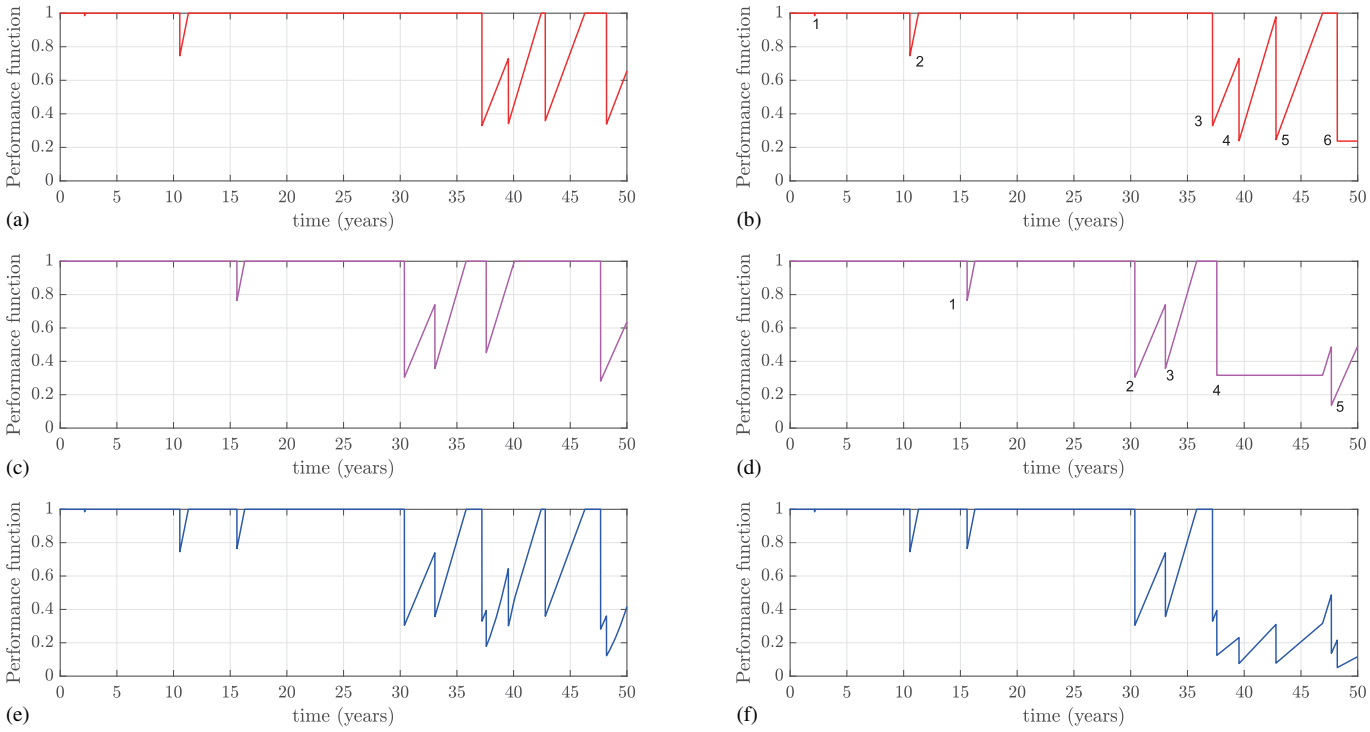

Fig. 5. Sampled performance functions considering Type 6 interaction and $\xi_h = 0.2$: (a) $Q_1(t)$; (b) $Q_1^*(t)$; (c) $Q_2(t)$; (d) $Q_2^*(t)$; (e) $Q_{\text{mul}}(t)$; and (f) $Q_{\text{mul}}^*(t)$.

nonresilience. For example, for a reference period of 50 years, the mean nonresilience equals 0.022, 0.033, 0.048, and 0.074 respectively corresponding to the four deterioration scenarios of $\mu_Q(t)$. The observations from Fig. 7 suggest the importance of incorporating the hazard nonstationarity in resilience assessment.

The impact of η_q on the mean nonresilience is revealed in Fig. 8 for a reference period of 50 years, with the same configuration as in Fig. 6 except η_q. While the variation of η_q does not affect the mean nonresilience if ignoring the performance function dependency, a greater value of η_q indicates a weaker correlation between $Q_1(t)$ and $Q_2(t)$, and thus results in smaller mean nonresilience for both Type 5 and 6 interactions.

The influence of performance dependency type on resilience is examined in Fig. 9 for a reference period of 50 years, considering the six types of interactions between $Q_1(t)$ and $Q_2(t)$. The configuration of the structure in Fig. 9 is as in Fig. 6, and Type 0 means independent performance functions. The mean nonresilience

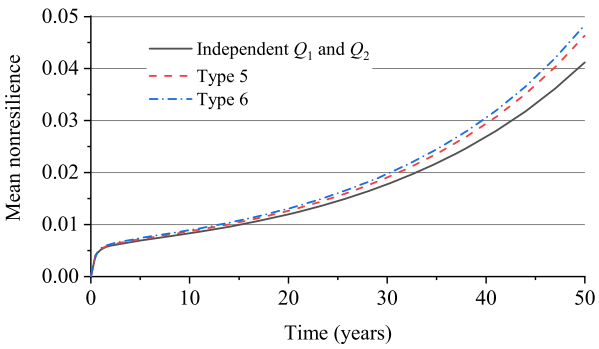

Fig. 6. Time-dependent mean nonresilience associated with Type 5 and 6 interactions.

associated with Type 0 is the smallest, because it has assumed independence between the two performance functions. This is consistent with the observation from Fig. 6. Further, partially considering the $Q_1(t)$–$Q_2(t)$ dependency also underestimates the mean nonresilience, as revealed through the comparison between Types 1, 2 (or 3, 4, or 5, 6). The mean nonresilience of Type 2 is greater than that of Type 4, due to the more critical effect of delayed recovery process on resilience. Moreover, the mean nonresilience associated with Type 6 is the largest, as it has fully incorporated the mutual dependency between the two performance functions.

Fig. 10 depicts the effect of posthazard recovery profile on mean resilience. The variation of ξ indicates different recovery rates of the posthazard functionality, as previously illustrated in Fig. 5, and thus has an essential impact on resilience. For both types of performance interaction, a smaller value of ξ means a less rapid recovery process, and thus leads to greater nonresilience. This is because of the enhanced interaction between $Q_1(t)$ and $Q_2(t)$, which is consistent with the comparison between Figs. 4 and 5. Correspondingly, for a fixed reference period, the difference between the mean nonresiliences considering independent or interacting performance functions becomes larger with a smaller ξ. Further, with a longer reference period, the impact of ξ on mean nonresilience is enhanced, due to the increasing number of hazardous events (and thus larger number of performance interactions).

Example 2: Resilience of a Building Subjected to Groundwater Intrusion and Hurricane Winds

In this section, the resilience problem of a virtual building located in Miami-Dade County, Florida (a coastal area) is examined. Two types of hazards will be considered: (1) groundwater intrusion leading to the deterioration of foundation loading bearing capacity; and (2) hurricane wind threatening the serviceability and safety of the

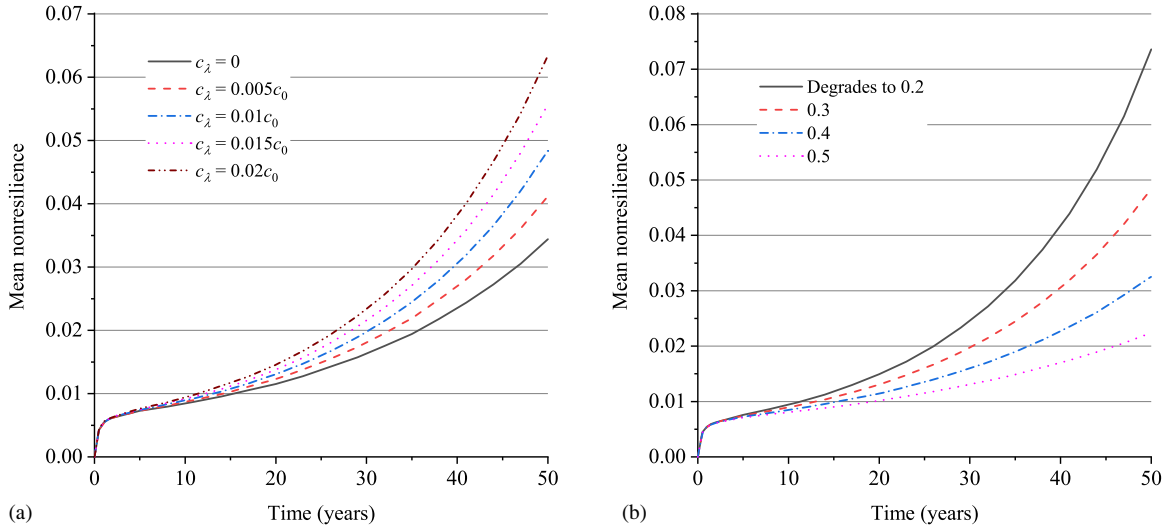

Fig. 7. Impact of hazard nonstationarity on time-dependent mean nonresilience: (a) impact of occurrence rate; and (b) impact of mean value of Q_r.

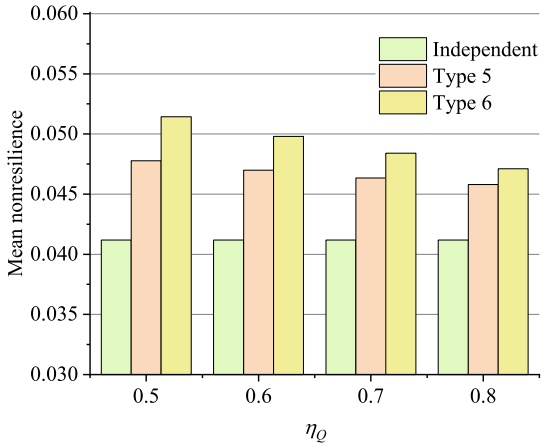

Fig. 8. Effect of η_Q on time-dependent mean nonresilience for $t_l = 50$ years.

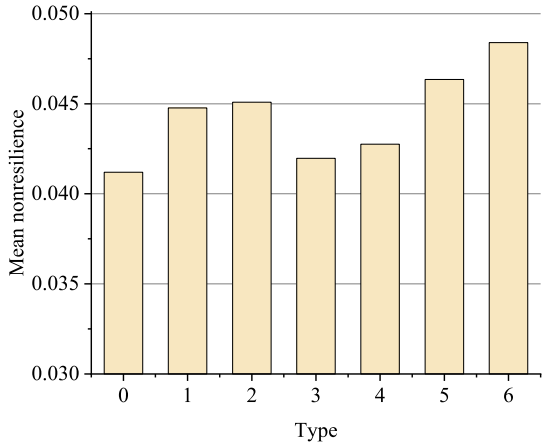

Fig. 9. Effect of performance interaction type on time-dependent mean nonresilience.

building. Assume that the building has a strip foundation with a width of 0.9 m and a depth of 0.6 m, as adopted from Wang et al. (2023) and illustrated in Fig. 11. The foundation is subjected to the impacts of groundwater intrusion due to sea level rise (SLR) in a changing climate. The load bearing capacity of the foundation, R_{ult}, can be determined by the trinomial formula as follows (Terazaghi 1943):

$$R_{\text{ult}} = cN_c + \gamma D_f N_q + 0.5\gamma B_f N_\gamma \tag{17}$$

in which c is the cohesion of soil, γ is the unit weight of soil, D_f and B_f are the depth and width of the foundation, respectively (Fig. 11),

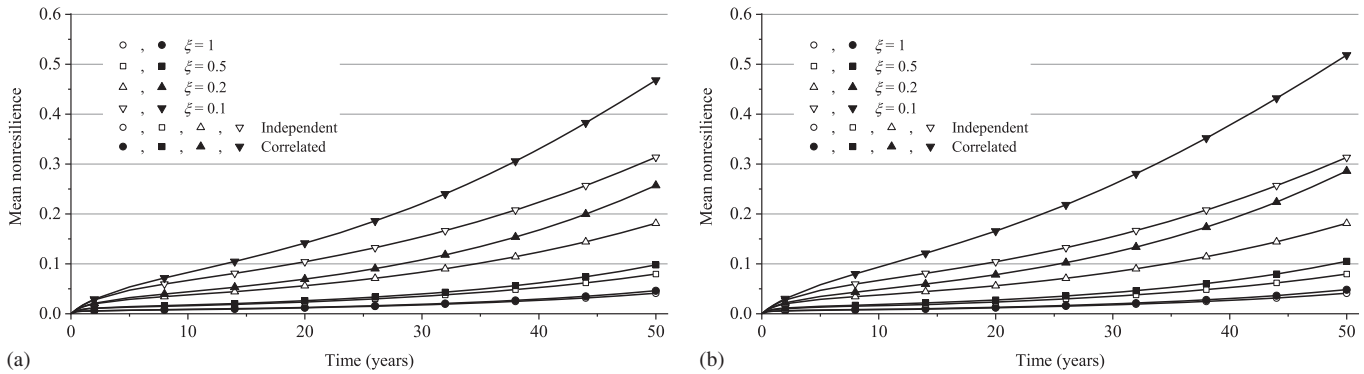

Fig. 10. Impact of recovery profile on time-dependent mean nonresilience: (a) Type 5; and (b) Type 6.

N_c, N_q, N_γ are functions of the soil internal friction angle ϕ, and are expressed as

$$N_q = \tan^2\left(\frac{\pi}{4}+\frac{\phi}{2}\right)\exp(\pi\tan\phi) \tag{18}$$

$$N_c = (N_q - 1)\cot\phi \tag{19}$$

$$N_\gamma = 2(N_q + 1)\tan\phi \tag{20}$$

Note that Eq. (17) holds when the groundwater table is below the foundation bottom with a minimum distance of B_f. Otherwise, one needs to adjust Eq. (17) to fit more general cases. If the groundwater table is above the foundation bottom at a distance of x_a (Case 1 in Fig. 11), Eq. (17) becomes

$$R_{\text{ult}} = cN_c + [\gamma(D_f - x_a) + x_a(\gamma_{\text{sa}} - \gamma_w)]N_q + 0.5(\gamma_{\text{sa}} - \gamma_w)B_f N_\gamma \tag{21}$$

in which γ_{sa} is the saturated unit weight of soil, and γ_w is the unit weight of water. If the groundwater table is below the foundation bottom at a distance of x_b (Case 2 in Fig. 11), Eq. (17) is rewritten as

$$R_{\text{ult}} = cN_c + \gamma D_f N_q + 0.5\left[(\gamma_{\text{sa}} - \gamma_w) + \frac{x_b}{B_f}(\gamma - \gamma_{\text{sa}} + \gamma_w)\right]B_f N_\gamma \tag{22}$$

The statistical information of the variables associated with the soil properties is summarized in Table 1 (assuming that the cohesion of soil is negligible). The initial groundwater table is 1.8 m lower the ground level. Further, taking into account the impact of climate change, the groundwater table will increase, as a result of SLR, by 0.5–1.4 m over 80 years. This will affect the load bearing capacity of the foundation, as revealed in Eqs. (21) and (22), and subsequently the serviceability. Assume that the performance function of the foundation decreases from 1 (at the initial time) to 0.8 upon R_{ult} degrading by 5%, and to 0.5 if R_{ult} degrades by 10%, with which the maintenance measure is conducted to restore the load bearing capacity to the initial state. The maintenance time is normally distributed with a mean value of two years and a COV of 0.2.

Next, the performance of the building exposed to hurricane winds is evaluated through comparing the wind speed and the generalized capacity, denoted by R, whose cumulative distribution function (CDF) has the same shape as the fragility curve (Wang et al. 2020). Typically, R is assumed to follow a lognormal distribution, with which the probability density function (PDF), $f_R(r)$, takes a form of

$$f_R(r) = \frac{1}{\sqrt{2\pi}r\nu_R}\exp\left[-\frac{1}{2}\left(\frac{\ln r - \kappa_R}{\nu_R}\right)^2\right], \quad r > 0 \tag{23}$$

where the two parameters κ_R and ν_R are the mean value and the standard deviation of $\ln R$, respectively, and are related to the mean value and the variance of R according to

$$\mu_R = \exp\left(\kappa_R + 0.5\nu_R^2\right); \quad \sigma_R^2 = \mu_R^2\left[\exp(\nu_R^2) - 1\right] \tag{24}$$

in which μ_R and σ_R^2 are the mean value and the variance of R, respectively.

In this example, four post-hurricane damage states for the building will be considered, namely, none, moderate, severe, and complete damage states. As a result, three generalized capacities are used in the damage assessment, denoted by R_1, R_2, and R_3 (note that each R has the same unit as the wind speed). These capacities have mean values of 49.24, 56.13, and 63.02 m/s, respectively, in terms of the gust wind speed, and an identical COV of 0.11. Corresponding to the four damage states, the remaining functionalities are 100%, 50%, 25%, and 0%, respectively, and the recovery times are 0, 120, 360, and 720 days (HAZUS 2003).

The occurrence of hurricane events is modeled by a Poisson process with an occurrence rate of $\lambda(t)$. Conditional on the occurrence of a hurricane event, the maximum wind speed, V, follows a Weibull distribution, and its CDF, $F_V(v, t)$ at time t, is as follows (Li et al. 2016):

$$F_V(v, t) = 1 - \exp\left[-\left(\frac{v}{u(t)}\right)^{\alpha(t)}\right] \tag{25}$$

in which v is the 1-minute average wind speed, and $u(t)$ and $\alpha(t)$ are the time-variant scale and shape parameters of the Weibull distribution. A conversion factor of 1.23 is used (Harper et al. 2010) to further convert V into the gust wind speed (as used in the aforementioned fragility curves). Through examining the historical data from 1901 to 2010, Li et al. (2016) calibrated the scale and shape parameters in Eq. (25) as 35.9 m/s and 2.06, respectively, for Miami-Dade County. The average annual number of hurricanes is 0.245 (27 events in a 110-year period). To further consider the impact of climate change on future hurricane events, the scale parameter and occurrence rate are modeled by time-variant functions as follows (with a fixed shape parameter of 2.06):

$$u(t) = 35.9 + c_1 t, \quad \lambda(t) = 0.245 + c_2 t \tag{26}$$

in which c_1 and c_2 are two constants reflecting the changing rates of $u(t)$ and $\lambda(t)$, respectively. Illustratively, the following four cases of hurricane hazard are considered in this example [based on Eq. (26)].

i. Case 1. Both the intensity (reflected through the scale parameter) and occurrence rate do not vary with time, yielding a stationary hurricane process.
ii. Case 2. The hurricane intensity increases by 50% over 80 years, with a time-invariant occurrence rate.

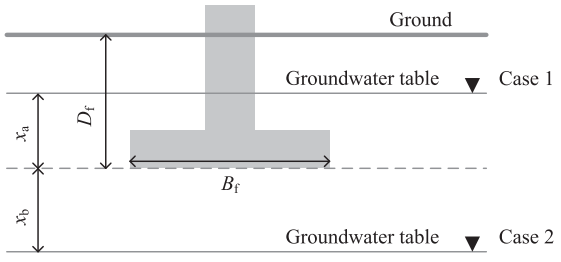

Fig. 11. Strip foundation.

Table 1. Statistics of the soil property variables

Variable	Mean	Coefficient of variation (COV)	Distribution type
Unit weight of soil γ	16 kN/m^3	0.15	Lognormal
Soil friction angle ϕ	30 °	0.10	Lognormal
Saturated unit weight of soil γ_{sa}	18 kN/m^3	0.15	Lognormal

Source: Adapted from Wang et al. (2023).

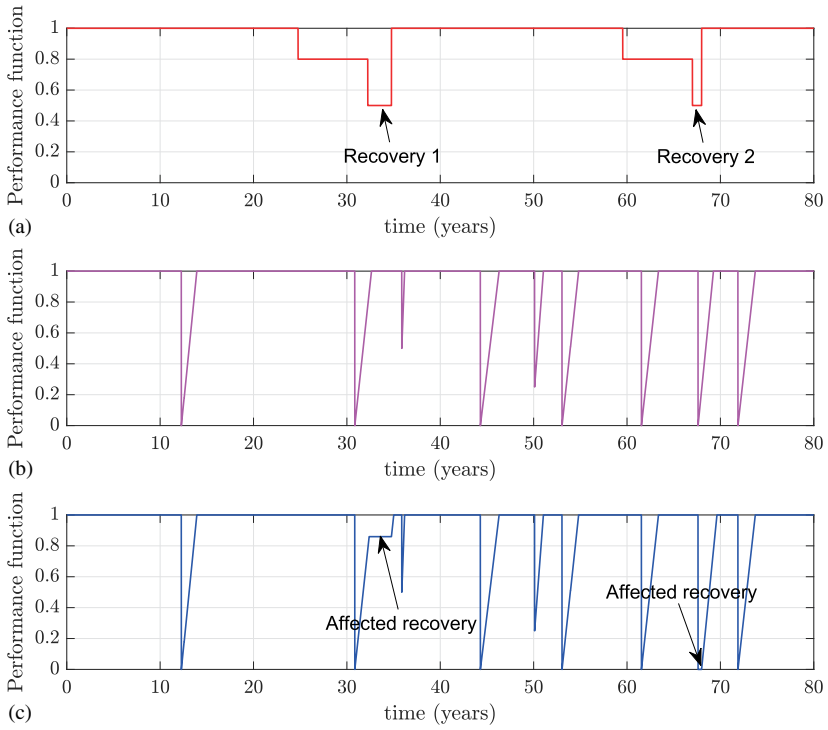

Fig. 12. Sample trajectories of a building's performance functions: (a) $Q_1(t)$; (b) $Q_2(t)$; and (c) $Q_2^*(t)$.

iii. Case 3. The hurricane occurrence rate increases by 50% over 80 years, with a time-invariant intensity.
iv. Case 4. Both the intensity and occurrence rate increase by 50% over 80 years.

Let $Q_1(t)$ and $Q_2(t)$ denote the hurricane- and groundwater intrusion-related performance functions, respectively. In terms of performance interaction, assume that the post-hurricane recovery process is postponed if another recovery associated with groundwater intrusion is in progress (this is similar to the Type 1 interaction in Example 1). A set of sampled trajectories for $Q_1(t)$, $Q_2(t)$ and $Q_2^*(t)$ is depicted in Fig. 12, showing that $Q_2^*(t)$ has been affected by two recovery processes associated with $Q_1(t)$.

The time-dependent mean nonresilience for reference periods up to 80 years is depicted in Fig. 13 (see the legend "Interacting"), assuming a 1.4-m groundwater table rise over 80 years and Case 4 hurricane scenario. The mean nonresilience assuming independent performance functions is also presented in Fig. 13, which is smaller than that incorporating the $Q_1(t)$–$Q_2(t)$ interaction. This is consistent with the observation from Fig. 6. For example, for a reference period of 80 years, the mean nonresilience is underestimated by 44.8% if ignoring the performance function interaction. Further, the difference between the mean nonresiliences associated with independent/interacting performance functions is negligible for reference periods up to 30 years, but becomes more significant for longer reference periods. The variation of the difference between the mean nonresiliences can be explained by examining the time of conducting the first and second maintenance measures against groundwater intrusion, denoted by T_1 and T_2, respectively. While there is a probability that no (5.9%) or only one (49.5%) maintenance measure is conducted through the reference period of 80 years, the conditional distributions of T_1 and T_2 on their existence, as depicted in Fig. 14, account for the amplified difference between the mean nonresiliences in Fig. 13 around 30 and 60 years, respectively.

An important feature of the resilience problem examined herein is that the groundwater table rise-induced hazard is not necessarily a Poisson process. As a result, existing resilience models assuming a Poisson process for the hazard occurrence (e.g., that in Wang et al. 2022) are not applicable in this context. This further demonstrates the applicability of Eq. (10) for general cases.

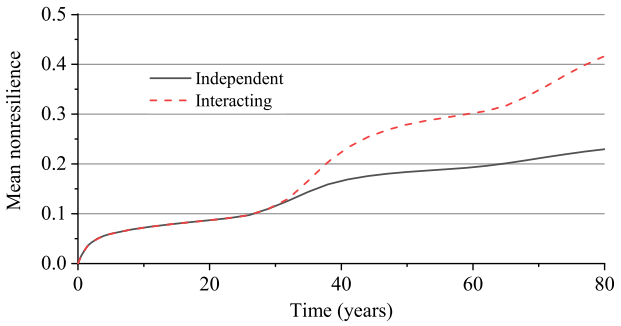

Fig. 13. Time-dependent mean nonresilience considering groundwater intrusion and hurricane hazards.

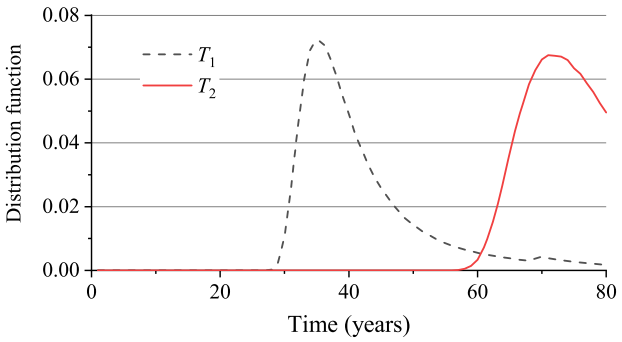

Fig. 14. Conditional probability distribution of the time of first/second restoration on existence.

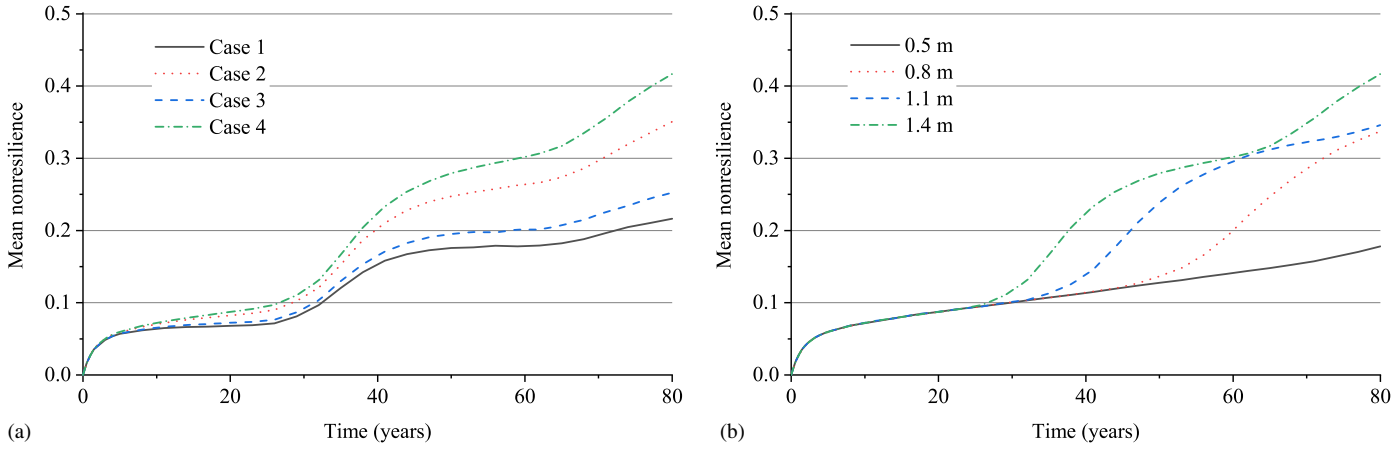

Fig. 15. Impact of hazard nonstationarity on time-dependent mean nonresilience of a building: (a) impact of hurricane scenarios; and (b) impact of groundwater table rise.

The impact of hazard nonstationarity in a changing climate on time-dependent mean nonresilience is examined in Fig. 15. In Fig. 15(a), the groundwater table rises by 1.4 m over 80 years. The mean nonresilience associated with Case 4 (i.e., both intensity and occurrence rate increase by 50% over 80 years) is the greatest, followed by those associated with Cases 2, 3, and 1. For instance, the mean nonresilience associated with Case 1 (0.216) is underestimated by 48.1% compared with Case 4. This observation indicates the importance of reasonably projecting the future changing scenarios of hurricanes in resilience assessment. In particular, the comparison between Cases 2 and 3 demonstrates that the mean nonresilience is more sensitive to the variation of future hurricane intensity than the occurrence rate. In Fig. 15(b), the groundwater table rises by 0.5, 0.8, 1.1, and 1.4 m respectively, while the Case 4 hurricane scenario is adopted. A more severe scenario of groundwater table rise due to SLR results in larger mean nonresilience, and thus a less resilient building. For example, for a reference period of 80 years, the mean nonresilience is 0.417 with the groundwater table rising by 1.4 m, which is underestimated by 57.3% if considering a 0.5 m rise of groundwater table. The difference between the mean nonresiliences associated with different groundwater rise scenarios does not vary monastically with time, because of the joint behavior of T_1 (and/or T_2) associated with different groundwater intrusion hazards.

Concluding Remarks

In this paper, a new method for the evaluation of time-dependent resilience has been developed, which takes into account the interaction between performance functions associated with different types of hazards. The proposed resilience model can also take into account the hazard nonstationarity in terms of the hazard intensity and/or occurrence rate due to the potential impacts of climate change. A novel concept of the PCI is proposed to develop further insights into the resilience problem. The following conclusions can be drawn from this paper.

1. The proposed resilience model is applicable for both discrete and continuous hazard processes, and takes into account the interaction between performance functions associated with different hazard types, reflected through the postponed recovery process if the recovery associated with the other hazard type is in progress, and/or the amplified hazard-induced performance reduction due to the nonfull performance associated with the other hazard type.
2. The proposed PCI, which takes a similar form of the Shannon information content (a concept in information theory), measures asset owner/decision maker's concern about the performance of an object (structure or infrastructure). An important feature of the proposed PCI is that, for two independent hazard types, the total amount of concern equals the sum of the concerns related to each hazard type.
3. The mean nonresilience, if close to zero, can be approximated by the mean value of the average PCI over the considered reference period. This observation suggests that one can interpret the mean nonresilience as the asset owner/decision maker's average concern on the life-cycle performance of an object.
4. The interaction between the performance functions associated with different types of hazards plays an essential role in resilience assessment. Ignoring such interaction underestimates the nonresilience (44.8% for the virtual building examined in Example 2), and thus yields a nonconservative estimate of the object's performance.
5. Resilience assessment needs to incorporate the time-variant characteristics of the hazard intensity and/or occurrence rate in a changing climate. Ignoring the impact of hazard nonstationarity underestimates the mean nonresilience by approximately 50%.

In future works, the resilience evaluation of complex infrastructure systems consisting of multiple interacting components is a promising topic, which requires the optimization of resource allocation that supports the recovery processes of multiple components, but has not been addressed in this paper.

Data Availability statement

All data, models, or code that support the findings of this study are available from the corresponding author upon reasonable request.

Acknowledgments

The research described in this paper has been jointly supported by the University of Wollongong (Vice-Chancellor's Postdoctoral Research Fellowship), the Federal Railroad Administration, and the

National Oceanic and Atmospheric Administration. These supports are gratefully acknowledged. The authors would like to acknowledge the thoughtful suggestions of two anonymous reviewers, which substantially improved the present paper.

References

Argyroudis, S. A., S. A. Mitoulis, M. G. Winter, and A. M. Kaynia. 2019. "Fragility of transport assets exposed to multiple hazards: State-of-the-art review toward infrastructural resilience." *Reliab. Eng. Syst. Saf.* 191: 106567. https://doi.org/10.1016/j.ress.2019.106567.

ATSE (Australian Academy of Technological Sciences and Engineering). 2022. "Building a resilient Australia." Retrieved August 22, 2023. https://www.atse.org.au/wp-content/uploads/2022/10/220930-ATSE-Position-Statement-Building-a-Resilient-Australia.pdf.

Attoh-Okine, N. O., A. T. Cooper, and S. A. Mensah. 2009. "Formulation of resilience index of urban infrastructure using belief functions." *IEEE Syst. J.* 3 (2): 147–153. https://doi.org/10.1109/JSYST.2009.2019148.

Ayyub, B. M. 2015. "Practical resilience metrics for planning, design, and decision making." *ASCE-ASME J. Risk Uncertainty Eng. Syst. Part A: Civ. Eng.* 1 (3): 04015008. https://doi.org/10.1061/AJRUA6.0000826.

Ayyub, B. M., and G. J. Klir. 2006. *Uncertainty modeling and analysis in engineering and the sciences*. Boca Raton, FL: CRC Press.

Ayyub, B. M., and R. H. McCuen. 2016. *Probability, statistics, and reliability for engineers and scientists*. Boca Raton, FL: CRC Press.

Bruneau, M., M. Barbato, J. E. Padgett, A. E. Zaghi, J. Mitrani-Reiser, and Y. Li. 2017. "State of the art of multihazard design." *J. Struct. Eng.* 143 (10): 03117002. https://doi.org/10.1061/(ASCE)ST.1943-541X.0001893.

Bruneau, M., and A. Reinhorn. 2007. "Exploring the concept of seismic resilience for acute care facilities." *Earthquake Spectra* 23 (1): 41–62. https://doi.org/10.1193/1.2431396.

CalMatters. 2023. "California officials respond to Tropical Storm Hilary, an Ojai quake and wildfires." Retrieved August 22, 2023. https://calmatters.org/newsletters/whatmatters/2023/08/california-tropical-storm-hilary.

Cimellaro, G. P., A. M. Reinhorn, and M. Bruneau. 2010. "Framework for analytical quantification of disaster resilience." *Eng. Struct.* 32 (11): 3639–3649. https://doi.org/10.1016/j.engstruct.2010.08.008.

Gerstenberger, M. C., et al. 2020. "Probabilistic seismic hazard analysis at regional and national scales: State of the art and future challenges." *Rev. Geophys.* 58 (2): e2019RG000653. https://doi.org/10.1029/2019RG000653.

Gidaris, I., J. E. Padgett, A. R. Barbosa, S. Chen, D. Cox, B. Webb, and A. Cerato. 2017. "Multiple-hazard fragility and restoration models of highway bridges for regional risk and resilience assessment in the united states: State-of-the-art review." *J. Struct. Eng.* 143 (3): 04016188. https://doi.org/10.1061/(ASCE)ST.1943-541X.0001672.

Goss, M., D. L. Swain, J. T. Abatzoglou, A. Sarhadi, C. A. Kolden, A. P. Williams, and N. S. Diffenbaugh. 2020. "Climate change is increasing the likelihood of extreme autumn wildfire conditions across California." *Environ. Res. Lett.* 15 (9): 094016. https://doi.org/10.1088/1748-9326/ab83a7.

Harper, B., J. Kepert, and J. Ginger. 2010. *Guidelines for converting between various wind averaging periods in tropical cyclone conditions*. WMO/TD-No. 1555. Geneva: World Meteorological Organization.

HAZUS. 2003. *Multi-hazard loss estimation methodology: Hurricane model*. Washington, DC: US Dept. of Homeland Security.

IPCC (Intergovernmental Panel on Climate Change). 2021. *Climate change 2021: The physical science basis*. Contribution of Working Group I to the Sixth Assessment Report of the Intergovernmental Panel on Climate Change. Cambridge, UK: Cambridge University Press.

Laurien, F., J. G. Martin, and S. Mehryar. 2022. "Climate and disaster resilience measurement: Persistent gaps in multiple hazards, methods, and practicability." *Clim. Risk Manage.* 37: 100443. https://doi.org/10.1016/j.crm.2022.100443.

Li, Q., C. Wang, and H. Zhang. 2016. "A probabilistic framework for hurricane damage assessment considering non-stationarity and correlation in hurricane actions." *Struct. Saf.* 59: 108–117. https://doi.org/10.1016/j.strusafe.2016.01.001.

Li, Y., Y. Dong, D. M. Frangopol, and D. Gautam. 2020. "Long-term resilience and loss assessment of highway bridges under multiple natural hazards." *Struct. Infrastruct. Eng.* 16 (4): 626–641. https://doi.org/10.1080/15732479.2019.1699936.

MacKay, D. J. 2003. *Information theory, inference and learning algorithms*. Cambridge, UK: Cambridge University Press.

McAllister, T. 2013. *Developing guidelines and standards for disaster resilience of the built environment: A research needs assessment*. Maryland: US Dept. of Commerce, National Institute of Standards and Technology.

Melchers, R. E., and A. T Beck. 2018. *Structural reliability analysis and prediction*. Hoboken, NJ: John Wiley & Sons.

Milkman, J. 1950. "Note on the functional equations $f(xy) = f(x) + f(y)$, $f(x^n) = nf(x)$." *Proc. Am. Math. Soc.* 1 (4): 505–508.

Ouyang, M., L. Dueñas-Osorio, and X. Min. 2012. "A three-stage resilience analysis framework for urban infrastructure systems." *Struct. Saf.* 36: 23–31. https://doi.org/10.1016/j.strusafe.2011.12.004.

Reed, D., C. Friedland, S. Wang, and C. Massarra. 2016. "Multi-hazard system-level logit fragility functions." *Eng. Struct.* 122: 14–23. https://doi.org/10.1016/j.engstruct.2016.05.006.

Risk and Resilience Measurement Committee. 2019. *Resilience-based performance: Next generation guidelines for buildings and lifeline standards*. Infrastructure Resilience Publication No. 3. Reston, VA: ASCE.

Salman, A. M., and Y. Li. 2017. "Multihazard risk assessment of electric power systems." *J. Struct. Eng.* 143 (3): 04016198. https://doi.org/10.1061/(ASCE)ST.1943-541X.0001688.

Salomon, J., M. Broggi, S. Kruse, S. Weber, and M. Beer. 2020. "Resilience decision-making for complex systems." *ASCE-ASME J. Risk Uncertainty Eng. Syst. Part B: Mech. Eng.* 6 (2): 020901. https://doi.org/10.1115/1.4044907.

Terazaghi, K. 1943. *Theoretical soil mechanics*. Hoboken, NJ: John Wiley & Sons. https://doi.org/10.1002/9780470172766.

Wahl, T., S. Jain, J. Bender, S. D. Meyers, and M. E. Luther. 2015. "Increasing risk of compound flooding from storm surge and rainfall for major us cities." *Nat. Clim. Change* 5 (12): 1093–1097. https://doi.org/10.1038/nclimate2736.

Walsh, K., C. J. White, K. McInnes, J. Holmes, S. Schuster, H. Richter, J. P. Evans, A. Di Luca, and R. A. Warren. 2016. "Natural hazards in Australia: Storms, wind and hail." *Clim. Change* 139: 55–67. https://doi.org/10.1007/s10584-016-1737-7.

Wang, C. 2021. *Structural reliability and time-dependent reliability*. Cham: Springer Nature Switzerland AG.

Wang, C. 2023a. "A generalized index for functionality-sensitive resilience quantification." *Resilient Cities Struct.* 2 (1): 68–75. https://doi.org/10.1016/j.rcns.2023.02.001.

Wang, C. 2023b. "Role of recovery profile dependency in time-dependent resilience." *Eng. Rep.* e12716. https://doi.org/10.1002/eng2.12716.

Wang, C., B. M. Ayyub, and A. Ahmed. 2022. "Time-dependent reliability and resilience of aging structures exposed to multiple hazards in a changing environment." *Resilient Cities Struct.* 1 (3): 40–51. https://doi.org/10.1016/j.rcns.2022.10.001.

Wang, C., B. M. Ayyub, and W. G. P. Kumari. 2023. "Resilience model for coastal-building foundations with time-variant soil strength due to water intrusion in a changing climate." *Rock Soil Mech.* 44 (1): 67–74.

Wang, C., M. Beer, and B. M. Ayyub. 2021. "Time-dependent reliability of aging structures: Overview of assessment methods." *ASCE-ASME J. Risk Uncertainty Eng. Syst. Part A: Civ. Eng.* 7 (4): 03121003. https://doi.org/10.1061/AJRUA6.0001176.

Wang, C., H. Zhang, B. R. Ellingwood, Y. Guo, H. Mahmoud, and Q. Li. 2020. "Assessing post-hazard damage costs to a community's residential buildings exposed to tropical cyclones." *Struct. Infrastruct. Eng.* 17 (4): 443–453. https://doi.org/10.1080/15732479.2020.1845215.

Xu, H., N. Lin, M. Huang, and W. Lou. 2020. "Design tropical cyclone wind speed when considering climate change." *J. Struct. Eng.* 146 (5): 04020063. https://doi.org/10.1061/(ASCE)ST.1943-541X.0002585.

Yin, Y.-J., and Y. Li. 2011. "Probabilistic loss assessment of light-frame wood construction subjected to combined seismic and snow loads." *Eng. Struct.* 33 (2): 380–390. https://doi.org/10.1016/j.engstruct.2010.10.018.